Synthesis and Mechanical Properties of $Na_{0.7}CoO_2$

A Thesis

Presented to the Faculty of the Graduate School

of Cornell university

in Partial Fulfillment of the Requirements for the Degree

of Master of Science

by

Yuanmeng Zhang

December 2017

Abstract

Materials comprised of large $Na_{0.7}CoO_2$ nanosheets were made through a novel nanomanufacturing technique. This technique is based on sol-gel processing followed by electric-field induced kinetic-demixing and high temperature calcination. Demixing conditions play a vital role in the sheet growth. Kinetic demixing under different temperatures (300–500ºC), electrical currents of 500 mA and 750 mA, and duration times between 0-60 hours were tested to establish relationships between kinetic demixing conditions and the length of sheets. An embedding and polishing method was developed for this fragile material. The hardness and reduced modulus of $Na_{0.7}CoO_2$ with nanolayered structure are reported for the first time based on nanoindentation tests. The correlation between the mechanical properties and the structure of the nanolayered materials is reported. A deformation mechanism for nanolayers is suggested based on layer sliding. Aging problems associated with this material are also reported for the first.

Biographical Sketch

Yuanmeng Zhang was born and raised in China. She attended University of Science and Technology Beijing for her undergraduate education and received a B.S. in Materials Science. She came to the United States and spent two meaningful years in Cornell University for her Master's study.

Acknowledgements

First and foremost, I want to thank my parents for their tremendous love and support. I would also like to thank my advisor, Dr. Shefford Baker, for his advice and guidance, as well as assistance in helping me see a bigger picture whenever I asked for help. I also want to thank him for giving me the opportunity to do research. I also want to thank Dr. Richard Robinson, who spent a great deal of time and resources on my project. Last, but certainly not least, I am very grateful to all the group members from Baker group and Robinson group, who have been there to help me overcome the technique problems with my experiments and give me valuable suggestions.

List of Contents

List of Tables

List of Figures

1. Introduction

Nanolayered materials consist of nanoscale two-dimensional plates weakly stacked to form three-dimensional structures, and they usually display a large anisotropy in their properties [1]. Nanolayered materials form strong chemical bonds in-plane but weak van der Waals bonding out-of-plane, so they are easy to exfoliate into nanosheets. Exfoliated nanosheets are usually known as two-dimensional (2D) materials. The most well-known 2D material is graphene, which was first exfoliated from van der Waals solids in 2004 [2-4]. Since then, research on other 2D materials beyond graphene has attracted attention and grown rapidly [5]. Even though most of these materials have not been widely used in commercial applications, many industries are paying close attention to them [6]. From graphite to MoS_2 and layered clays, these nanolayered materials display a wide range of electronic, electrochemical, magneto-optical, ferromagnetic, thermoelectric, mechanical and catalytic properties [7-11].

As one of the nanolayered materials, Na_xCoO_2 has been a material of high interest since 1996 when its unusual thermoelectric properties were first discovered [12]. Thermoelectric oxides are of high interest due to the promise of applications in electronic devices. It's a major societal problem to provide a sustainable supply of energy. Thermoelectric materials can transform a temperature difference into an electric potential, or create an electric potential from a temperature difference. Thermoelectric oxides could play a vital role in meeting the energy

challenge we are facing today. Na_xCoO_2 has the advantages of being non-toxic, light, and cheap, which makes it a promising cathode material for use in sodium ion batteries [13]. Indeed, it is suggested that Na_xCoO_2 cells may challenge the lithium-ion counterparts [14-16]. Na_xCoO_2 has a thermoelectric figure of merit ZT = 1.2 at around 800 K [17]. The Seebeck coefficient of bulk Na_xCoO_2 is reported to be around 100 μV/K, which indicates a p-type thermoelectric material. Its metallic conductivity is reported to be 5000 S/cm [12, 18].

Recently, large $Na_{0.7}CoO_2$ nanosheets displaying flexibility during mechanical bending were discovered [19]. If this discovery is true, the combination of mechanical deformable and great thermoelectric property of $Na_{0.7}CoO_2$ can lead to many applications like biosensors and flexible electronics, just like MoS_2 and graphene which shares these two properties [20-24]. To confirm the deformability of the layers, we employed nanoindentation to make indents, and examined the layer deformation with SEM. The nanosheets here are only 10 to 100 nm thick, and nanoindentation is perfect for testing on small-scale sample. The hardness and elastic modulus of $Na_{0.7}CoO_2$ are reported for the first time.

Since previous studies have not reported about the flexibility of $Na_{0.7}CoO_2$ nanosheets, we hypothesize that longer nanosheets are more flexible. In our work, Aksit's method of fabricating extremely long nanoscale-thick $Na_{0.7}CoO_2$ nanosheets [19] is modified. This method is the only one that reports the fabrication of nanosheets up to 1.8 mm long, while other methods generally produce sheets with lengths of less than 10 μm. This new method is based on sol-gel processing followed by electric-field induced kinetic-demixing, and has the advantage of being environmentally friendly, easy, and cheap. Compared to traditional methods such as spark plasma sintering (SPS) and solid state reactions (SSR), this method also has the advantage of

fabricating a sintered body with high crystallographic orientation and desirable thermoelectric properties. To test the best parameters to synthesize layers with maximized length, the impact of temperature, amount of electric current, and duration of electrically induced kinetic demixing on the morphology is studied.

In the second chapter, we describe previous studies related to this material and theory basics for our experiment. In the third chapter, all the methods used in our experiments are recorded in detail. In the fourth chapter, we will show all the experiment data and discuss them. In the conclusion part, we will summarize our work.

2. Background

2.1. Na_xCoO_2

$Na_{0.7}CoO_2$ is a material with 2D crystalline structure. In 1997, it was discovered to be a material with very good thermoelectric properties [12]. This discovery has prompted intensive research about Na_xCoO_2 [25]. In 1999, Ray *et al*. [26] found a special localized Curie-Weiss magnetism in Na_xCoO_2, which was believed to be existent only in insulators. This discovery proved that magnetism can coexist with metallic behavior. In 2003, Takada *et al*. [27] discovered that superconductivity occurs after hydration of Na_xCoO_2. Water penetrates between the CoO_2 layers and Na layers, separating the layers. This separation seems to lead to superconductivity for Na_xCoO_2 with $0.28 < x < 0.37$ with the critical temperature T_c between 4.3 K and 4.8 K. The superconducting properties are very similar to the superconductivity of layered copper oxides, suggesting that the two systems may share similar underlying physics.

Four different phases have been reported in Na_xCoO_2 [28]. There is α phase when $0.5 < x < 0.6$, α' phase for $0.5 < x < 0.7$, β phase for $0.9 < x < 1$, and γ phase for $x \sim 0.7$. Different phases of Na_xCoO_2 have different structures. According to Yakabe *et al*. [29], The structure of Na_xCoO_2 strongly depends on the sodium content. Even though they all share the same two-layer Na_xCoO_2 system, they have different crystal structure. For example, when $x = 0.92$ and 0.32, Na_xCoO_2 is

trigonal with Na in octahedral coordination. $Na_{0.5}CoO_2$ has a monoclinically distorted single-layer structure. $Na_{0.6}CoO_2$ has a single-layer unit cell and is found to be isostructural with $Na_{0.6}CoO_2$ [30]. $Na_{0.7}CoO_2$ has a complex crystal structure. It has a layered structure composed of CoO_2 layers with Na layer in between as shown in Fig. 2.1. Each CoO_2 layer forms an edge-sharing CoO_2 octahedral network.

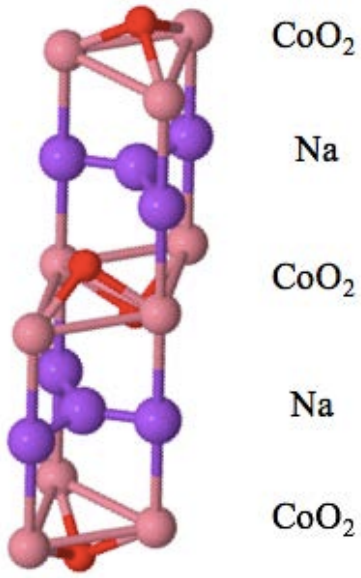

Fig. 2.1 A unit cell of $Na_{0.7}CoO_2$

The degree of filling of the Na between CoO_2 layers controls the charge in the CoO_2 planes, resulting in different properties as a function of x [31-33]. It is reported that Na_xCoO_2 with $x > 0.5$ has Curie-Weiss metal properties. For $x < 0.5$, it has paramagnetic properties, and for $x = 0.5$, it behaves like a charge-order insulator. Despite the popular belief that oxides have poor thermoelectric performance, the γ phase ($x \sim 0.7$) of Na_xCoO_2 shows a large Seebeck coefficient, metallic conductivity, and excellent thermoelectric properties, which makes it a promising cathode material for use in sodium ion batteries [13]. Indeed, it has been suggested that

$Na_{0.7}CoO_2$ cells may challenge the lithium-ion counterparts [14-16]. $Na_{0.7}CoO_2$ has a thermoelectric figure of merit *ZT* = 1.2 at around 800 K. The Seebeck coefficient of bulk $Na_{0.7}CoO_2$ is reported to be around 100 μV/K, reaching the industrial standard Bi_2Te_3 [34]. Its metallic conductivity is reported to be 5000 S/cm [17,18].

Despite the high *ZT* value, large $Na_{0.7}CoO_2$ sheets are reported to be flexible after mechanical bending in Aksit's work [19]. This is worth our attention because oxides are usually brittle, and it makes them difficult to shape, thus creating a geometric restriction when fitting in a heat device. A deformable thermoelectric material can solve this problem. Na_xCoO_2 nanosheets displaying flexibility during mechanical bending are reported for the first time in Aksit's work.

2.2. Synthesis of Na_xCoO_2

Current understanding of the synthesis processes of $Na_xCoO_2$is very poor. The conventional solid state reactions (SSR) method [35] is very complex, requiring the precursor materials to be ball milled before firing. This method also fails to fabricate a sintered body with the desired microstructure and high crystallographic orientation. The compositional inhomogeneity in the matrix in samples made by the SSR method leads to deterioration of the thermoelectric performance. Other methods such as spark plasma sintering (SPS) [36], polymerized complex (PC) and citric acid complex (CAC) methods [37] are also utilized in the synthesis of $Na_{0.7}CoO_2$, but are only able to produce small grains.

Recently, a new method of producing nanostructured thermoelectric oxides $Na_{0.7}CoO_2$ was reported by Aksit *et al*. [19]. He reported that this method can produce nanosheets with thicknesses around 10-100 nm and length around 1.8 mm. $Na_{0.7}CoO_2$ produced in this method has a very good thermoelectric property as high as the industry standard. This synthesis employs

the sol-gel process and E-field kinetic demixing, and produces $Na_{0.7}CoO_2$ with a layered structure. The layered structure is shown in Fig. 2.2. The layers are reported to be millimeter long, and display flexibility during mechanical bending [19].

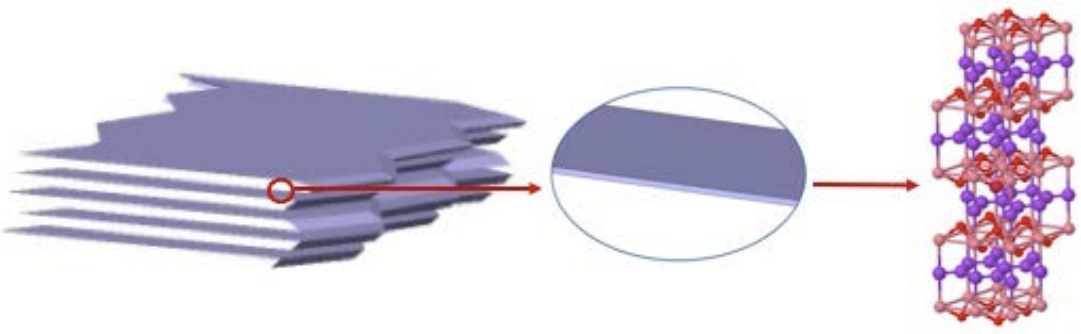

Fig. 2.2 The structures of the stacking of the $Na_{0.7}CoO_2$ layers

Aksit's method is highly dependent on E-field kinetic demixing. In an initially homogeneous solid solution, for example $(A_xB_{1-x})O$, kinetic demixing is a process used to enrich A or B on one crystal side. This enrichment process is caused by a driving force generated from a thermodynamic potential gradient, which can be a gradient of temperature [38], oxygen [39-42], stress [43], or electrical potential [44]. As a result of the driving force, fluxes of the chemical components will occur. Compositional changes can severely change the structure of the materials, and alter their properties. The first kinetic process is studied by Schmalzried *et al.* [39, 40] for $(Co_xMg_{1-x})O$ in a gradient of oxygen potential. Due to the difference of mobility between Co and Mg, the faster cation, Co, becomes enriched on one side of the crystal. The first E-field kinetic demixing was conducted by Monceau *et al*. [44] They analyzed the charge and

diffusivities of the cations in the process of kinetic demixing of cations in semiconducting oxides and in ionic conductors.

In Aksit's method, demixing is a critical step to enrich Na in one side of the crystal. The E-field kinetic-demixing provides a driving force for sodium and cobalt to move due to the electric potential difference. However, under controlled temperature, Co has a much lower mobility than Na. As a result, only Na would be driven to flow to one side while Co stays stationary. In most experiments, it is common to use a constant current instead of a constant voltage since the field strength is highly unstable due to the changes in the microstructure of the sample between the probes [45]. The demixing process separates the pellet into Na-rich and Na-depleted regions, and clear boundaries can be observed on the pellet. Three factors are very important during the demixing process: temperature, electric current, and duration of the demixing process.

The temperature of demixing is crucial since temperature can change the electrochemical mobility of Na and Co. As explained before, the mobility difference between Na and Co is the reason they can be separated. When the temperature is relatively low, the mobility of Co is significantly lower than that of Na [46]. Low temperature (~300ºC) guarantees that demixing happens successfully during kinetic-demixing, but also has the drawback of taking longer to complete. A study by Ohta *et al*. [47] reported that Co is still stationary as long as the temperature is less than 600ºC. In this work, temperatures including 300ºC, 400ºC, and 500ºC are used to test the influence of high temperature on the outcome of demixing. Increasing temperature would speed up the movement of Na, but would increase the risk of driving Co to one side. A balance between efficiency and structure integrity needs to be maintained by testing the influence of temperature on the structure.

Phase separation is not only controlled by temperature but also pressure. Tsori's study [48] shows that within a time limit, once the applied voltage reaches a critical value, the higher the potential difference between two sides of the sample, the more the cations would be enriched near the anode. The critical currents are below 500 mA for $Na_{0.7}CoO_2$ according to Aksit's study [19]. In most experiments, the currents applied in E-field kinetic demixing are controlled to less than 1.5 A due to the small volume of sample size [49]. Size of samples synthesized in this work is also very small, so the currents used were set to 500 mA and 750 mA.

Cation redistribution during demixing is also time dependent according to Monceau's study [44]. The cationic current density keeps increasing until it reaches a constant value over time. Aksit [19] reported his demixing was complete after 48 hours of demixing. However, no one has studied what happens to the structure of the materials if the applied currents don't terminate after the demixing is done. In order to study the time-dependent demixing process, the duration is also set differently to explore the effect of demixing duration on nanosheets growth in our experiment. Samples are demixed for four different durations: 0, 24, 48 and 60 hours.

2.3. Mechanical properties of nanolayered structure $Na_{0.7}CoO_2$

$Na_{0.7}CoO_2$ synthesized in Aksit's method displays nanolayered structures [19]. Nanolayered materials have nanoscale thick two-dimensional layers weakly stacked to form three-dimensional structures, and display a wide range of electronic, optical, mechanical and electrochemical properties. These materials may play an important role in the development of engineering applications [50]. Structures consisting of layers have been mostly reported in biological materials such as nacre and bones [51-55], and the toughness brought by their layered structure inspires scientists to fabricate materials with similar structure [56]. There are many families of

layered materials. The most well-known one is graphite, which consists of multiple layers of graphene [57-59]. The third family is transitional metal dichalcogenides (TMDs) and metal halides. Their metal atoms are in between planes of halide/chalcogen atoms. The fourth family is the layered metal oxides (Na_xCoO_2, MnO_2, MoO_3 and $LaNb_2O_7$) [19, 60-64], and layered double hydroxides (LDHs). Layered double hydroxides (LDHs) are assembled via layer-by-layer (LBL) method, and an interesting magneto-optical response is reported in the multilayer films [65]. Another big family of layered material is clays [66-71]. Layered silicate clay such as montmorillonite displays a greatly improved mechanical properties of nylon 6/clay nanocomposites [72].

To explore the mechanical properties of $Na_{0.7}CoO_2$ nanosheets, nanoindentation is employed. Nanoindentation has become one of the most popular techniques in the determination of the mechanical properties of thin films, small volumes, and other small microstructural specimens on a nanoscale regime [73-77]. In 1900, The first standardized indentation test was designed by Brinell [78]. He used a very hard spherical indenter made of steel, and defined the Brinell hardness as the applied load divided by the surface area of the indent left on the sample surface. In 1908, Meyer suggested that the surface area used for hardness in Brinell's theory should be the "projected area" [79], which is still the commonly used measure for hardness today. Later, other tests like Vickers, Knoop, and Rockwell hardness test were developed [80]. The indenters they used were conical and pyramidal indenters, which are still commonly in use in modern experiments. Until then, indentation experiments had been mainly used for hardness measurement of a material. In 1992, Oliver and Pharr introduced an improved technique for determination of hardness and elastic modulus. This technique is widely accepted and has

become the most common method to analyze data obtained from modern commercial nanoindenters [66].

The method of Oliver and Pharr [81] is used to analyzed the indentation load-displacement data. An indenter is pressed into a material, causing both elastic and plastic deformation. After the indenter is removed, elastic displacement is recovered and the remaining displacement is the plastic deformation. A cross section of an indentation and parameters used in the analysis are shown in Fig. 2.3.

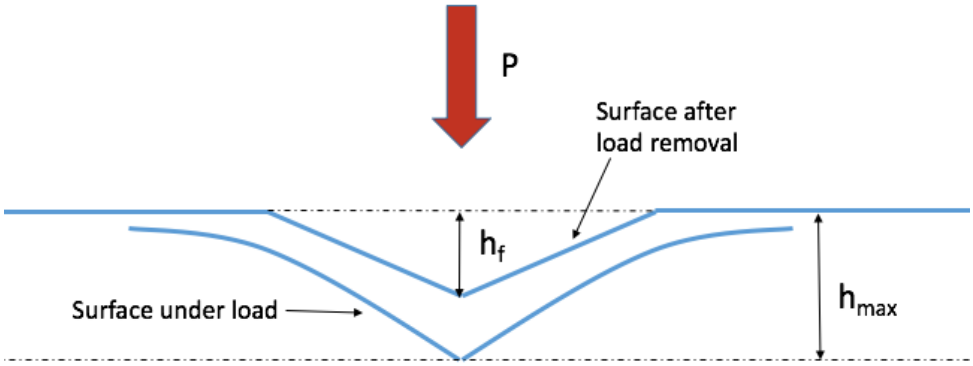

Fig. 2.3 A schematic representation of a section through an indentation.

Under the assumption that the deformation is elastic when unloading, and that the compliances of the sample and of the indenter are to be combined as reduced modulus E_r:

$$\frac{1}{E_r} = \left(\frac{1-v_i^2}{E_i}\right) + \left(\frac{1-v_m^2}{E_m}\right) \quad (1)$$

where E_i is the Young modulus for indenter, E_m is the Young modulus for tested material. v_i and v_m are the Poisson ratios for indenter and tested material. With these assumptions, we can model the contact:

$$s = \frac{2}{\sqrt{\pi}} E_r \sqrt{A} \quad (2)$$

where *S* is the unloading stiffness, and *A* is the contact area. This equation is fundamental in the calculations of hardness and modulus. Then the loading-unloading curve is fitted into a power law relationship:

$$P = \alpha(h_{max} - h_f)^m \quad (3)$$

where *P* is the load, m is a parameter related to the shape of indenter, h_f is the final depth, h_{max} is the total displacement.

Given that the indenter does not deform significantly, the contact area is $A_c = f(h_c)$. Then the hardness can be obtained as follows:

$$H = \frac{P_{max}}{\mathrm{A}} \quad (4)$$

Even though layered materials have been widely studied, there are not many studies about the mechanism of layer deformation. A “Tablet sliding” mechanism proposed by Barthelat is the most accepted one to explain the deformation of nacre layers [82]. Nacre is made of inorganic and organic layers. Researchers believe that the tablet would slide away under the indenter. In Barthelat’s study, they found “pop-in” effects, which are sudden displacement jumps in the load-displacement curve. They concluded that the “pop-in” event was due to the collapse and densification of the tablet interfaces during the tablet sliding process. They believe that the sheets are unable to effectively dissipate the accumulating load and start to slide under this force. A “tablet sliding” mechanism can’t explain the deformation of layers since a tablet and layer have different lateral extent. However, the similarity between sliding phenomenon of tablets and sliding of layers gives us an inspiration to come up with a new mechanism for layer deformation.

3. Experimental

3.1. Specimen preparation

3.1.1. Synthesis of $Na_{0.7}CoO_2$

The synthesis of $Na_{0.7}CoO_2$ follows a slightly modified version of Aksit's method [19]. A Flow chart of the procedure is shown in Fig. 3.1.

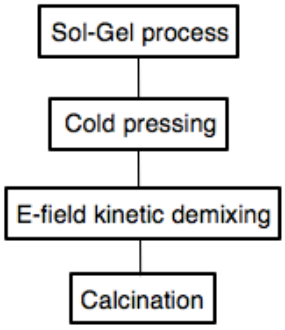

Fig. 3.1 Flow chart for the method used to prepare the $Na_{0.7}CoO_2$

Appropriate quantities of sodium nitrate, cobalt nitrate hexahydrate and poly (acrylic acid) are dissolved in de-ionized water to create an aqueous solution. The ratio of Na to Co is set to 0.72. Poly (acrylic acid) (PAA, average molecular weight M~ 1800 g/mol) is added to the solution

such that the ratio of PAA carboxylate groups to metal ions is 1:2. The sol-gel process is shown in Fig. 3.2. The solution is stirred using a magnetic stir bar on a hot plate with a temperature of 150ºC for 24 hours. After 24 hours, the color of the solution changes from pink red to dark red, and the remaining solution is 20% of the initial volume. The remaining solution is very viscous, indicating the formation of an aligned PAA-metal complex. The choice of the PAA is very critical. The metal cations can only be stabilized by the chelating groups through dipole forces between water molecules and metal ions. This is called “polymeric entrapment” or “steric entrapment” [83].

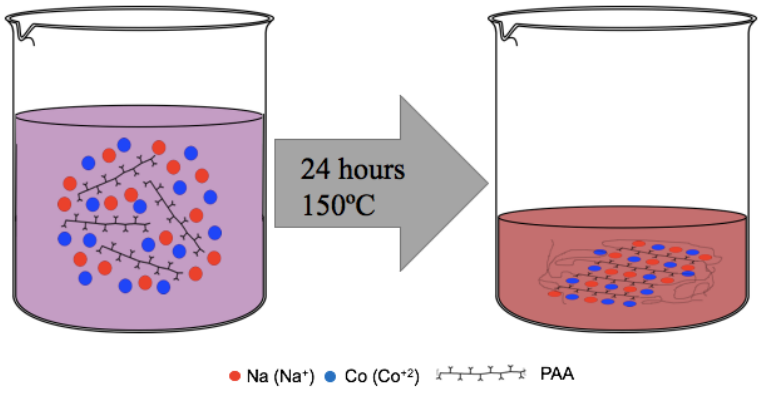

Fig. 3.2 A schematic diagram for the sol-gel process

The dark red solution is then poured into an aluminum foil container, and transferred into a furnace to be autocombusted at 500ºC. The powder formed after autocombustion is shown in Fig. 3.3. The organic compound (PAA) is pyrolyzed, but the molar ratio between Na and Co in the gel-solution is maintained during this process. The resulting mixture is a fluffy black powder composed of uniform metal oxide mixture with Co_3O_4 and CoO crystals [19], which is then uniaxially pressed into a 10 x 6 x 5 mm (Length x Width x Height) pellet in a stainless steel

rectangular die set. Before pressing, XRD data shows that the flakes are Co_3O_4 crystals with a relatively minor amount of CoO. After pressing, the cobalt oxide phases are still there, but there are signs of emergence of a Na_xCoO_2 phase.

Fig. 3. 3 Fluffy black powder in an aluminum foil container after autocombustion at 500ºC.

To concentrate the sodium on the cathode side, a constant electrical current is passed through the pellet through two copper plates with contacts made of silver epoxy. The E-field kinetic-demixing provides a driving force for sodium to move due to the electric potential difference. Demixing starts at room temperature, and is increased to the chosen temperature. Under room temperature, the current supply is in constant voltage (CV) mode with a voltage limitation of 21 V. Because of the high resistivity of the sample at room temperature, the current flowing through the sample is close to 0 A As the temperature increases and approaches 300ºC, the current dramatically increases and soon reaches the set current. When the current reaches its peak, The mode changes from CV to constant current (CC). Over the course of demixing the voltage would fluctuate between 2 - 21 V and decrease towards the end of the process. The demixing process separates the pellet into Na-rich and Na-depleted regions, and clear boundaries can be

observed on the pellet. A schematic figure of demixing process is shown in Fig. 3.4. The Na-rich part has darker color and higher density, while the Na-depleted part is light and porous. The parts are separated easily under pressure. In order to find the best condition to form long $Na_{0.7}CoO_2$ nanosheets, we need to find best conditions for demixing. We changed three conditions in demixing process: temperature, electric currents, and duration of the demixing process.

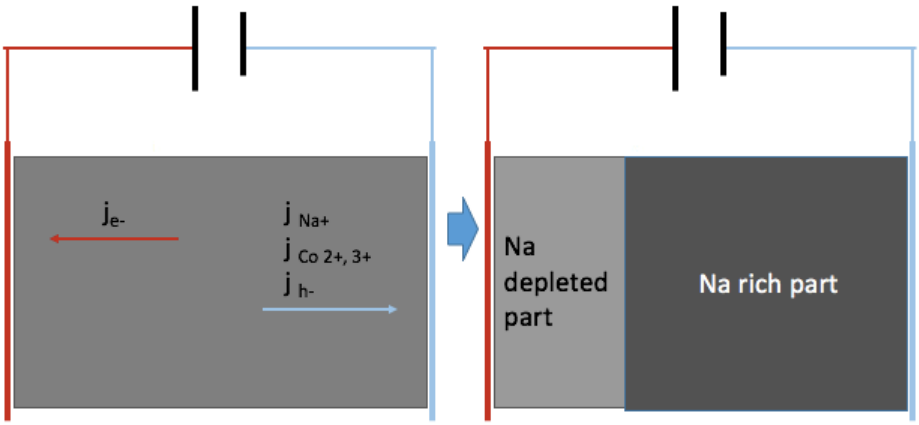

Fig. 3.4 Schematic diagram for E-field kinetic demixing. After the sol-gel process, the resulting black powders are pressed into a pellet.

In this work, temperatures including 300ºC, 400ºC, and 500ºC are used to test the influence of high temperature on the outcome of demixing. Samples were prepared at each of two demixing currents: 500 mA and 750 mA. The duration of demixing is controlled. Samples are demixed for four different duration: 0, 24, 48 and 60 hours. Duration changes the completeness of demixing. The relationship between completeness of structure of $Na_{0.7}CoO_2$ is tested.

After demixing is done, the pellet is divided into Na-rich and Na-depleted regions. The Na-depleted region is very porous and fragile, and easy to be separated from the other region. The Na-rich region of the pellet is placed on gold wires and heated up in a furnace to form

nanosheets. The furnace is rapidly heated to 1030ºC and maintained for 15 minutes. The pellet is then slowly cooled to 1000ºC in 90 mins. Once it reaches 1000ºC, the furnace is rapidly cooled down to room temperature. Because the pellet is rich in sodium due to the demixing process, extra heat treatment to obtain the thermoelectric stoichiometry (x = 0.7) is conducted. To obtain the thermoelectric phase of $Na_{0.7}CoO_2$, the sample is then held at 875ºC for ~30 hrs. After the second treatment, the pellet is mechanically removed from the gold wire using a razor blade. Residue on the wires can be removed by heating the wires in a 30 ml solution of 10 vol% hydrochloric acid for a few hours.

3.1.2. Measuring the layer length

The goal of the synthesis process is to produce nanosheets that are millimeter sized, so layer length is the most important parameter to determine the quality of the synthesis process we used in this experiment.

Measuring the layer length is done under the SEM. The sample used for SEM is half of the whole sample, which is gently separated from the whole sample with a razor blade. The magnification is the smallest in the beginning so the parts with obvious layer structure are observed. The surface was evenly divided into nine sections as shown in Fig. 3.5, and each section is about 100 μm x 100 μm. Every section was searched to find the layer-like structure. Then the area with layer-like structure was zoomed in to nanoscale to confirm the nanolayer structure. Nanolayers are layers with nanoscale thickness (10-100 nm), and each stack of nanosheets is at least few micrometers thick. Under the large magnitude, both ends of the layer were marked, and layer length is measured based on the two marks. The maximum layer length

in each section was recorded. They were averaged and reported as the maximum length of the sample.

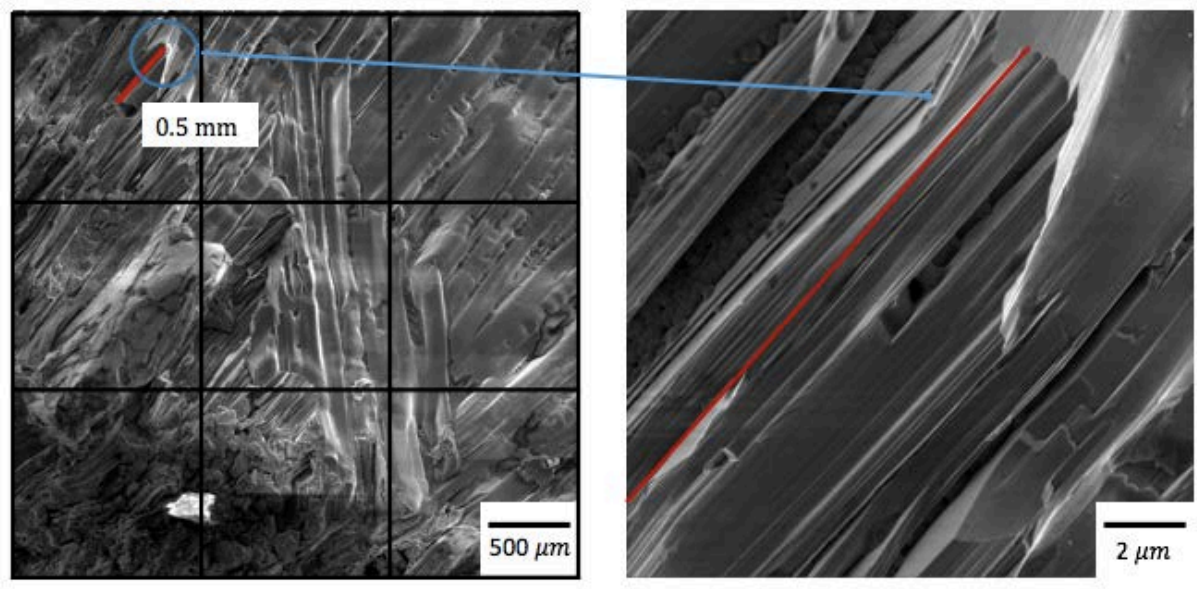

Fig. 3.5 Measuring the layer length. First the whole surface was observed under low magnitude, and divided evenly to nine sections. Find the longest layer-like stacks and zoom in to confirm its nanolayered structure.

3.1.2. Embedding and polishing

Each sample is embedded in an epoxy and left to dry for at least 24 hours. After the epoxy is dry, it is glued using a small drop of Loctite 401 on the AFM stub. The sample is then firmly pressed for at least 60 s to ensure that it is flat against the surface and that the glue is properly dried. The polisher is calibrated while the glue dries.

Before polishing, the specimen is mounted onto the parallel polishing sample holder. The first step is to place the round steel parallel polishing sample holder on a hot plate with temperature of 160ºC for 3 mins. When the holder is hot, small piece of crystalbond adhesive is placed on the center of the parallel polishing sample holder to melt. After the crystalbond adhesive becomes a viscous liquid, the sample holder is removed from the hot plate with tongs. The AFM stub with

the sample on the center of the sample holder is placed on the center of the holder. The sample is pressed firmly for at least 20 s to squish out excess crystalbond adhesive to make sure that the AFM stub is flat against the polishing sample holder. The crystalbond adhesive is allowed to cool down under room temperature for 5 mins.

The polishing starts with 30 μm sandpaper. The parallel polishing sample holder with a sample attached in the center is attached to the polishing head. It is important to turn on the polishing wheel and water and zero the front micrometer before lowering the vertical position cam to avoid causing damage to the sample surface. The sample is polished with the polishing wheel speed of less than 60 RPM until extra epoxy is removed and the sample surface is exposed. The sample is then treated the same with diamond paper with higher grit. The process is repeated with 15 μm, 9 μm, 5 μm, 3 μm, 1 μm, and 0.5 μm diamond paper. The key of polishing this fragile sample to avoid peeling of the layers is to slow down the wheel speed and increase the duration of polishing.

The final polish is done on polishing cloth using 0.02 colloidal silica spray for at least 2 hours. The last 1 minute is to be done with water to rinse off the silica. After the polishing is done, the sample is cleaned in an ultrasonic cleaner for few seconds to avoid damaging the sample. The sample holder is then placed onto hot plate again to allow the crystalbond to melt. The AFM stub is removed from the hotplate carefully. After the AFM stub is cooled down, crystalbond residue on the back of AFM stub is wiped off with acetone.

3.2. Mechanical properties characterization

3.2.1. Nanoindentation test

The mechanical properties of the bulk $Na_{0.7}CoO_2$ materials were characterized using nanoindentation with a Berkovich indenter tip. The shape of the sample is recorded in notes to help with finding the indents under SEM. Before the sample is put into the nanoindenter, it is carefully observed under optical microscope to make sure the sample is relatively flat and smooth.

A multiple loading-unloading function is used for the testing of $Na_{0.7}CoO_2$ samples. The loading function is shown in Fig. 3.6. The advantage of this loading function is the capability to investigate how hardness and modulus vary with the depth of the indenter in the sample. The technique allows the software to obtain hardness and modulus data at different depths in the sample in just one indent cycle. The load-holding segment is to prevent the inaccuracy the hardness measurement in case there is high time-dependent deformation in $Na_{0.7}CoO_2$.

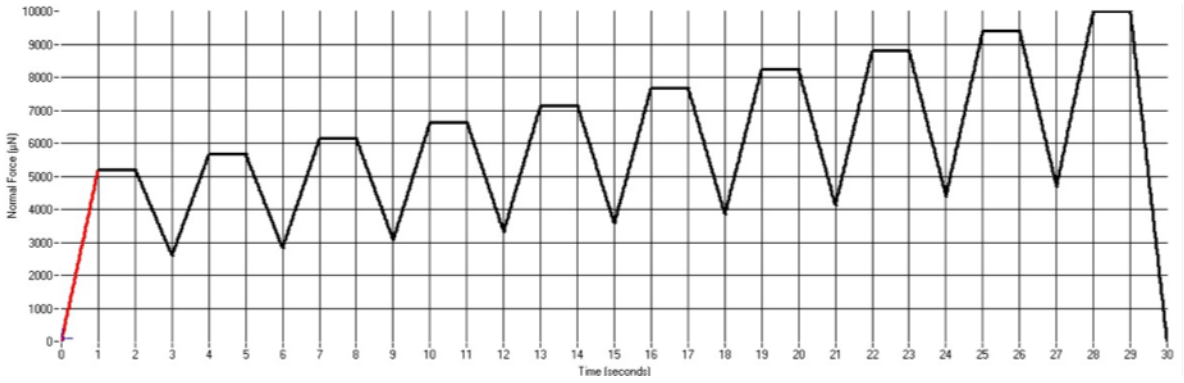

Fig. 3.6 The loading function used for the experiment

For this test, 25 indents were made on each sample with a pattern of 5 x 5 shown in Fig. 4.6.

Each indent is 10 μm away from another to prevent disruption. All the indentations made on the samples are at the maximum load (10,000 μN).

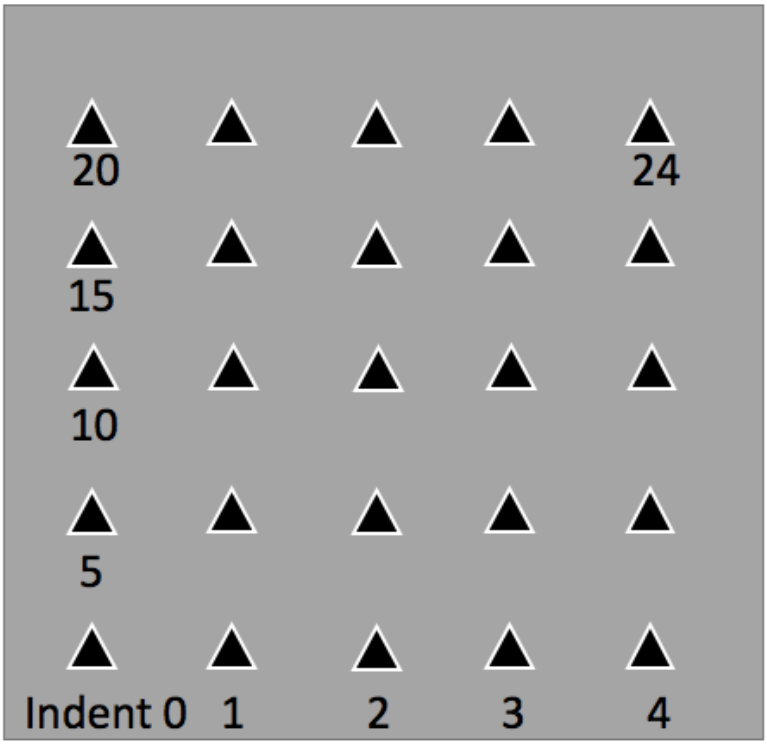

Fig. 3.7 The indentation pattern used in this experiment. The indent starts from the left corner, and move to the right. Then the indenter comes back to the left and repeats the path.

3.2.2. Data analysis of hardness and modulus

The hardness and modulus are obtained with Oliver-Pharr method [80]. Because of the multiple loading-unloading functions used for the test, for each indent, there are 25 datasets for hardness and 25 datasets for modulus. To filter out the data that doesn't meet the conditions required by the assumptions of the nanoindentation data analysis, the morphology of $Na_{0.7}CoO_2$ materials were examined using a scanning electron microscope (SEM). From the image, the indents on the edge of the sample, or on a crack, or on a rough surface would be picked out from the recorded

datasets. The mean and standard deviation is calculated from the remaining data, and used as the E/H result for each sample.

4. Results and Discussion

4.1. Synthesis and Morphology

Demixing is the key step in the synthesis of $Na_{0.7}CoO_2$ in this experiment. The parameters in E-field kinetic demixing process applied individual sample are summarized in Table 4.1. After synthesis, the samples were examined in SEM.

Table 4. 1 Sample naming, experimental parameters of demixing conditions

Sample no.	Demixing Temp [ºC]	Demixing Currents [mA]	Demixing Time [h]
1	300	500	48
2	400	500	48
3	500	500	48
4	300	750	24
5	300	750	48
6	300	750	60
7	N/A	N/A	N/A

4.1.1. Effect of Demixing Temperature on $Na_{0.7}CoO_2$ Morphology

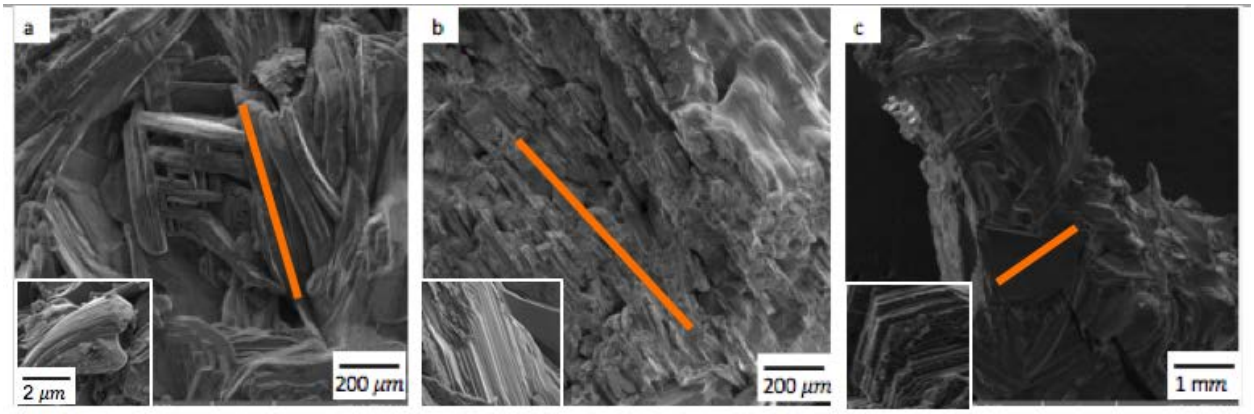

Fig. 4.1 SEM images of $Na_{0.7}CoO_2$ synthesized at different demixing temperature. Orange lines indicates the longest layer in the image. (a) SEM image of a sample demixed under 500 mA for 48 hours at 300ºC. (b) SEM image of a sample demixed under 500 mA for 48 hours at 400ºC. (c) SEM image of a sample demixed under 500 mA for 48 hours at 500ºC.

Fig. 4.1 shows SEM images of $Na_{0.7}CoO_2$ nanosheets synthesized under different demixing temperatures. The small images on the bottom left corner are the zoom-in image to confirm the layered structure. Samples shown here are sample No. 1, 2 and 3 according to Table 4.1. Sample currents were applied to them for the same time. Samples were observed under SEM, and their maximum layer lengths were measured by the methods explained before. All three samples showed layered structure, but with varied lengths. Nanosheets with ~0.5 mm in length were prepared at 300ºC. Sheets were longer (~ 0.7 mm) if the temperature was raised to 400ºC. There was an increase in sheet length when the demixing temperature reached 500ºC. $Na_{0.7}CoO_2$ produced at 500ºC has a length of over 1 mm.

Even though it seems true that high temperature during demixing is beneficial for layer growth, there is a risk of damaging the nanolayered structure when temperature is too high. Fig.

4.2 shows the nanolayered structure of these three samples mentioned above. When the demixing temperatures are below 400ºC, the thickness of layers formed are nanoscale. However, layers presented in Fig. 4.2c have thickness in micrometer scale. When the demixing temperature reaches 500ºC, the thickness of the layers becomes much larger than the layers from other samples.

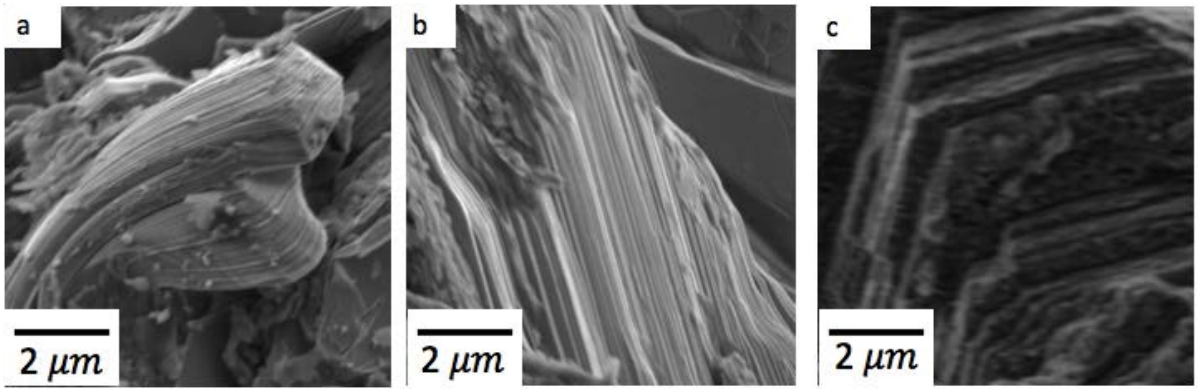

Fig. 4.2 SEM images of $Na_{0.7}CoO_2$ layers synthesized at different demixing temperature. (a) A sample demixed under 500 mA for 48 hours at 300ºC. (b) A sample under 500 mA for 48 hours at 400ºC. (c) A sample demixed under 500 mA for 48 hours at 500ºC.

An increase in temperature leads to layer growth within a certain temperature range. This is due to the increased mobility of Na at higher temperature. Increased mobility leads to more Na in the Na-rich side of the pellet.

The failure to form desired nanolayered structure (thickness 10-100 nm) in relatively high temperature (500ºC) can be explained by the increase of mobility of Co in $Na_{0.7}CoO_2$ at high temperature. As explained before, E-field induced kinetic demixing drives the cations move towards the cathode. However, the cations don't move as free ions in multicomponent metal oxides. Instead, they move by forming new metal oxides at cations through eq. (5):

$$n(Me^{\alpha+}_{Me^{\alpha+}})^x + \frac{m}{2}O_2(g) \rightarrow Me_nO_{m\,surf} + n(V_{Me^{\alpha+}})^{\alpha'} + n\alpha \quad (5)$$

Me is a metal, V is vacancy, and h is hole.

The reverse reaction happens at the anode side. As a result of this chemical reaction, many vacancies are formed at the cathode side. Both Co and Na want to occupy the vacancies, but the one with larger mobility would fill in most of the vacancies. Temperature would increase the mobility of both cations. At low temperature, Co would stay stationary. However, it starts to move relatively fast at 500ºC and occupy the vacancies that Na would have occupied at low temperature. Lack of Na results in the failure in forming nanolayered structure in $Na_{0.7}CoO_2$.

4.1.2. Effect of Demixing Currents on $Na_{0.7}CoO_2$ Morphology

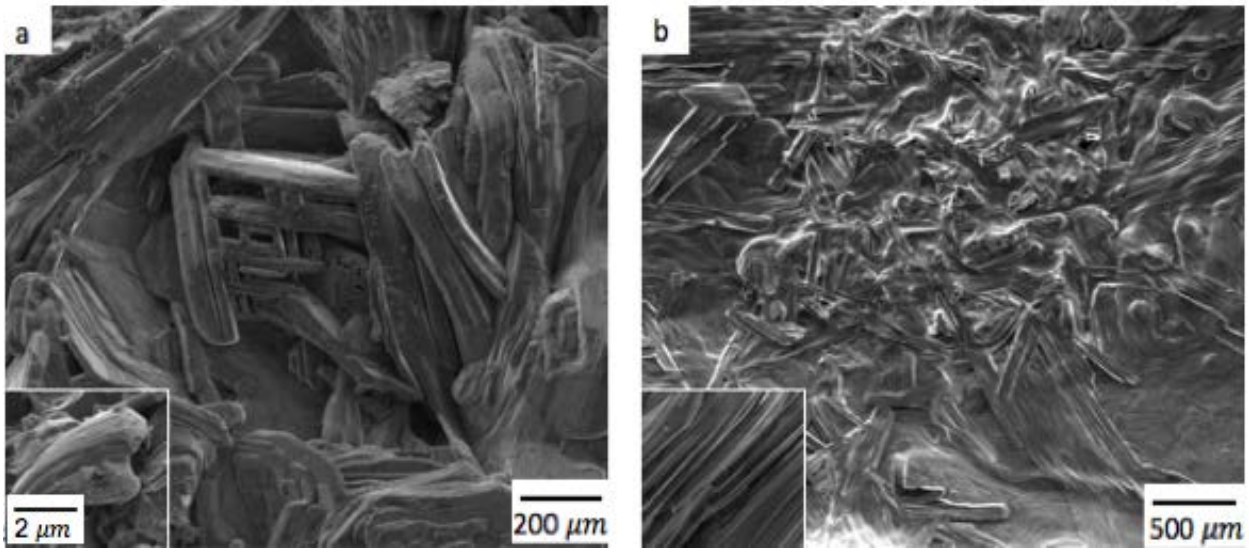

Fig. 4.3 SEM images of $Na_{0.7}CoO_2$ nanosheets under different demixing currents. (a) SEM image of a sample demixed under 500 mA for 48 hours at 300ºC. (b) SEM image of a sample demixed under 750 mA for 48 hours at 300ºC.

Nanosheets formed under different currents are shown in Fig. 4.3. Samples used here are sample No. 2 and No. 6 according to table 4.1. Fig. 4.3a showed the sample synthesized under slightly

lower currents (500 mA). Fig. 4.3b showed the one under 750 mA. All samples synthesized under both currents had layered structure, which is a sign for effective demixing. When the current of the kinetic demixing process was set to 500 mA, nanosheets in length no longer than 500 μm were observed. After increasing the current to 750 mA, the length reached 1.5 mm.

The reason that high currents would lead to growth in layers is that it gives more energy to cations. Higher currents mean higher voltage applied on the sample, the energy induced by E-field would increase as the voltage increases. The cations in $Na_{0.7}CoO_2$ are not free cations, and they need energy to liberate from O^{2-}. A higher current gives more energy and thus results in more Na in the Na-rich part of the pellet, and also helps with the sheet growth in the following calcination process.

4.1.3. Effect of Demixing Duration on $Na_{0.7}CoO_2$ Morphology

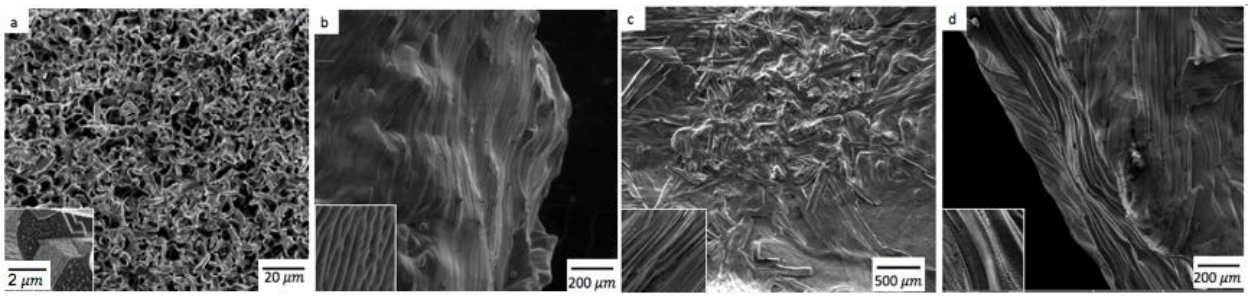

Fig. 4.4 SEM images of $Na_{0.7}CoO_2$ of different kinetic-demixing duration. (a) The sample which was not demixed does not have nanosheets structure, but instead flake-like structure. (b) The sample has been demixed under 750 mA at 300ºC for 24 hours. (c) The sample has been demixed under 750 mA at 300ºC for 48 hours. (d) The sample has been demixed under 750 mA at 300ºC for 60 hours.

The results of synthesis of $Na_{0.7}CoO_2$ under different duration time are shown in Fig. 4.4. The samples were demixed under the same conditions except for their demixing duration, which varied between 0 and 60 hours. Fig. 4.4 shows the SEM images of these samples. Fig. 4.4a

shows a sample with no demixing, and Fig. 4.4d shows a sample after 60 hours of demixing process.

As shown from Fig. 4.4a, the first sample (non-demixed) was very different from the other samples which have been demixed. Instead of a layered structure, the sample was made of small flakes and very porous. This suggested that increasing the ratio of Na:Co is critical in the layer growth.

The other three samples which have undergone kinetic demixing process demonstrated different nanosheet length with varied demixing duration. According to Fig. 4.4b, $Na_{0.7}CoO_2$ nanosheets with ~ 1 mm in length were observed when the duration of kinetic demixing was 24 hours. The length of nanosheets reached its maximum length ~ 1.5 mm when the demixing duration was 48 hours. Samples demixed for 60 hours did not show additional growth in sheets length. The length of the sheets increases with increased kinetic demixing duration.

Besides change in the layer growth, the nanolayer morphology also changes when the demixing duration is changes. The nanolayer morphology is shown in Fig. 4.5. Without demixing, instead of nanosheets, micro-size flakes are found in Fig. 4.5a. As demixing duration increase, morphology also changes. In Fig. 4.5 b and c, nanosheets are observed, but the distance between layers are different. Increasing demixing time beyond 48 hours does not make much difference in the sheet growth, but leads to dramatic change in nanolayer morphology. Instead of flat nanosheets, the nanosheets formed after 60-hour demixing are zig-zag like.

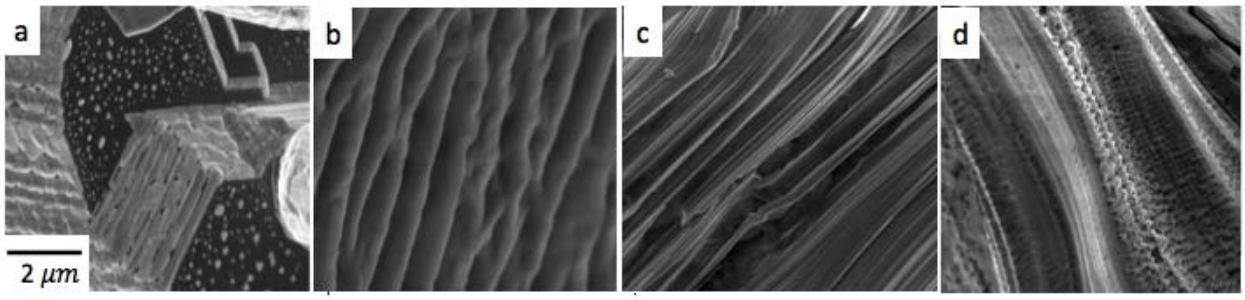

Fig. 4.5 SEM images of $Na_{0.7}CoO_2$ layers synthesized at different demixing temperature. (a) The sample which was not demixed does not have nanosheets structure, but instead flake-like structure. (b) The sample has been demixed under 750 mA at 300ºC for 24 hours. (c) The sample has been demixed under 750 mA at 300ºC for 48 hours. (d) The sample has been demixed under 750 mA at 300ºC for 60 hours.

Demixing is a time-consuming process. It takes time for the reaction which generates vacancy shown in eq. (5) to happen. Demixing is over when all the Na cations move to one side. Before the demixing duration hits a critical point, the molar ratio of Na:Co keeps growing, from the beginning 0.7 to over 1.3 at the end [19]. However, after the critical point is reached, increasing the duration would lead to structure change to nanolayer. Similar reports are not found in other literature. A possible explanation is that after almost all the Na has move to the Na-rich part, the lattice structure in Na-rich part would change, leading to movements of Co or O under applied voltage.

4.2. Delamination of Layers during Mechanical Polishing

Fig. 4.6. shows the layer is delaminated from the neighboring layer during mechanical polishing if the polisher speed is relatively high. This indicates the weak bonding between the layers and fragility of the structure. Fig. 4.6a shows a piece of small layer delaminated from the surface. And more small pieces are about to fall apart on the background. Fig. 4.6b shows a more detailed

image of how layers fall apart from each other. The delamination starts by forming cracks on the surface, and the layer gradually fall apart from the stack.

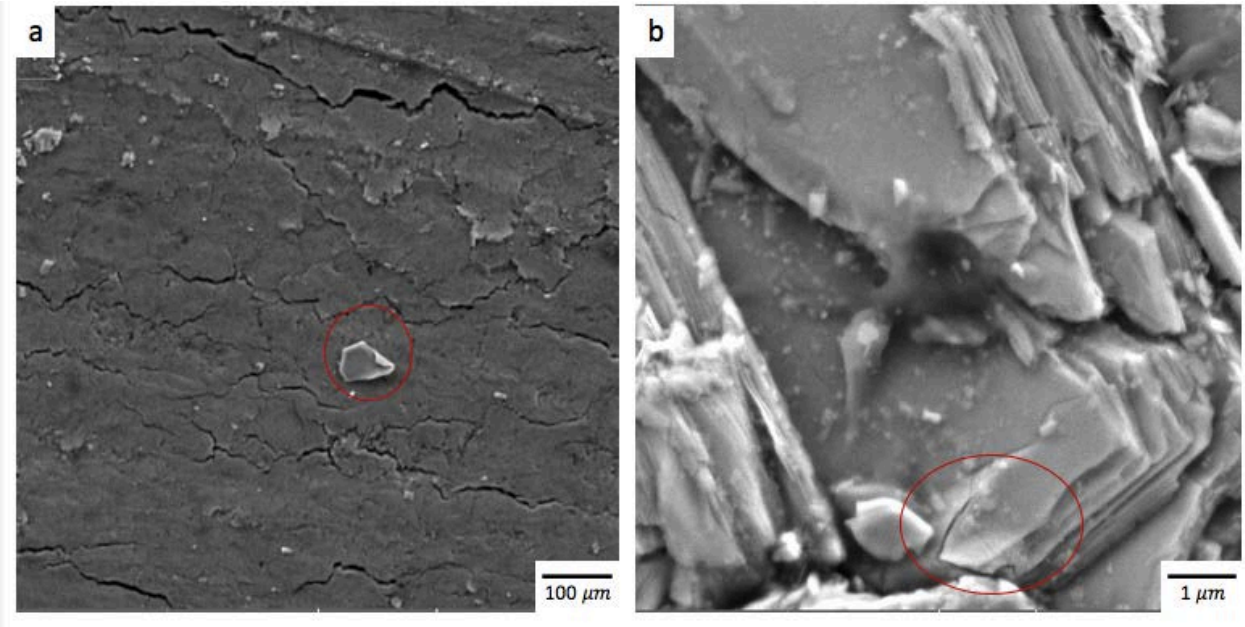

Fig. 4.6 Delamination of layers

4.2. Structure and Mechanical Properties

4.2.1. Layer Length and Mechanical Properties

A plot of hardness to layer length is shown. The shortest length is around 20 μm. This is the sample which has not been demixed. Other samples are all demixed under different conditions, and their lengths are mostly around 0.5 mm and 1.5 mm. The plot shows no obvious relationship between hardness and the length of the layers. No matter if the length of the layer is 20 or 1500 μm, the hardness of most samples fall into the range between 1.25 and 2 GPa. However, there are two samples that are not within this range.

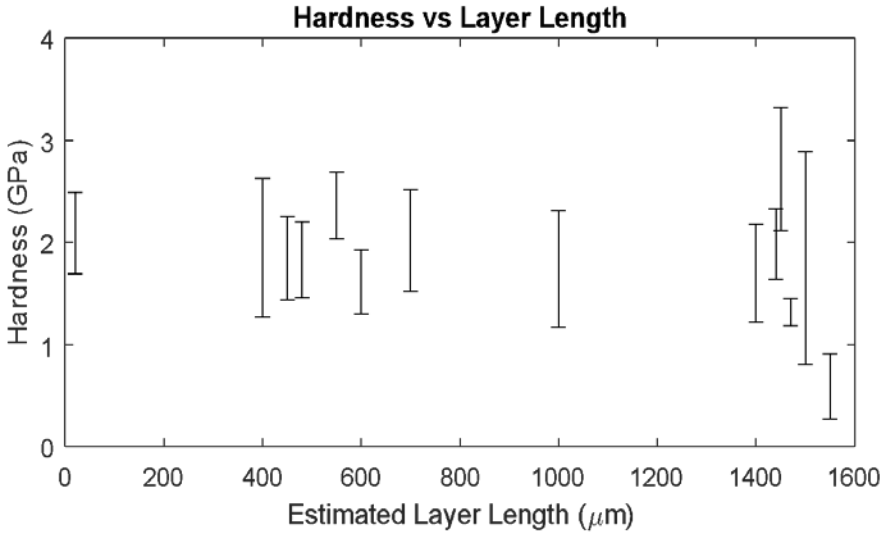

Fig. 4.7 A plot showing the relationship between the layer length and hardness

4.2.2. Aging of $Na_{0.7}CoO_2$

Table 4. 2 Sample Preparation (demixing conditions) and hardness

Temp [ºC]	Currents [mA]	Time [h]	Hardness [GPa]
300	500	48	1.61 ± 0.311
*300	*500	*48	2.36 ± 0.324
400	500	48	1.74 ± 0.57
500	500	48	1.85 ± 1.04
*500	*500	*48	0.59 ± 0.32
300	750	24	1.83 ± 0.37
300	750	48	1.7 ± 0.48
N/A	N/A	N/A	2.09 ± 0.4

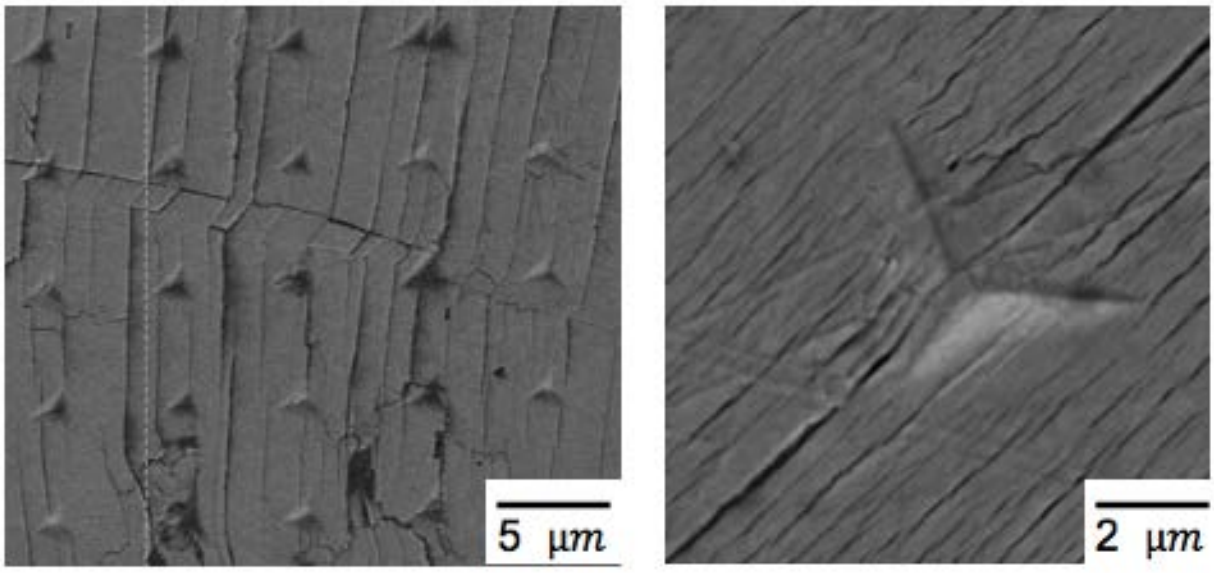

Fig. 4.8 SEM image of two samples with very high hardness (left) and very low hardness (right)

To understand why the two samples are special, the SEM images of the “extremely soft” and “extremely hard” samples surface are shown in Fig. 4.8. These two samples were prepared as shown in Table 4.1 (marked with *). The one with small crack has a small hardness (0.6 GPa), and the other one has a very large hardness (2.4 GPa). Instead of flat surfaces, the two special samples both show cracks on the surface. The cracks are both formed in one direction, but one sample has small cracks, the other has big ones. A typical load-displacement curve in Fig. 4.9 of the cracked samples shows creeping effect, which is increased penetration depth after the unloading segment begins, even though the load is decreasing. This means that the material creeping rate is higher than the unloading rate. The creeping effect can be seen by the occurrence of a round shape of the data (a ‘nose’) in the load-displacement curve. In this material, the creep effect can be explained by the propagation of the cracks during the unloading segment.

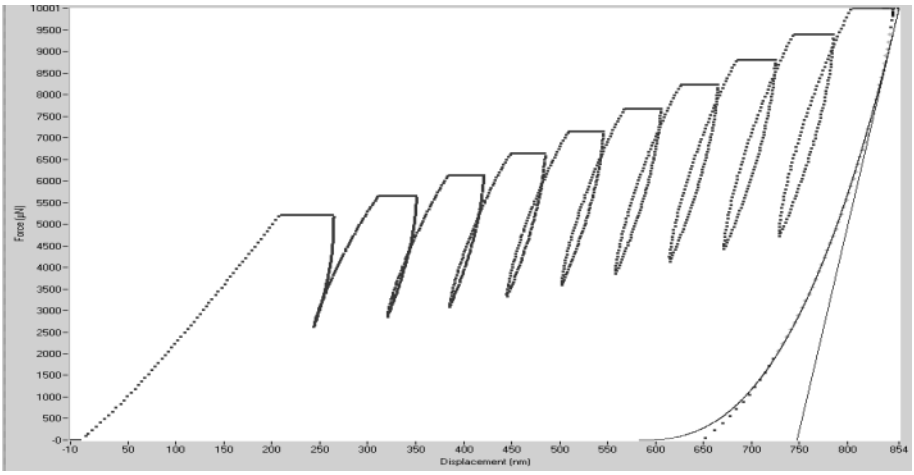

Fig. 4.9 Creeping effect observed from the load-displacement curve from indents on aging samples.

Cracks in materials have a huge influence on the mechanical properties. There is no clear answer as to why the materials have cracks. After carefully referring to the lab notes, we found that both the materials were made at least three months before the indentation tests. This finding draws our attention to the aging of the material.

Aging in material is very common. For $Na_{0.7}CoO_2$, two aging steps are observed as shown in Fig. 4.10: the first step is formation of cracks, the second is unknown material growth on the surface. The destruction of the structure is shown by the delamination of the layers. The second stage of aging in $Na_{0.7}CoO_2$ is the growth of unknown material on the surface. Under SEM, the unknown material is first observed as small dots, which slowly propagate and occupy the whole surface. Even from a micro image in Fig. 4.11, the influence of aging is very obvious. The surface of a new sample is black, and after a couple of months the unidentified white material is begins to form on top of the surface. After a year, the whole surface turns to white. The unknown material grown on the surface is not dissolvable in acetone, water, nor alcohol, but it is easily mechanically polished off.

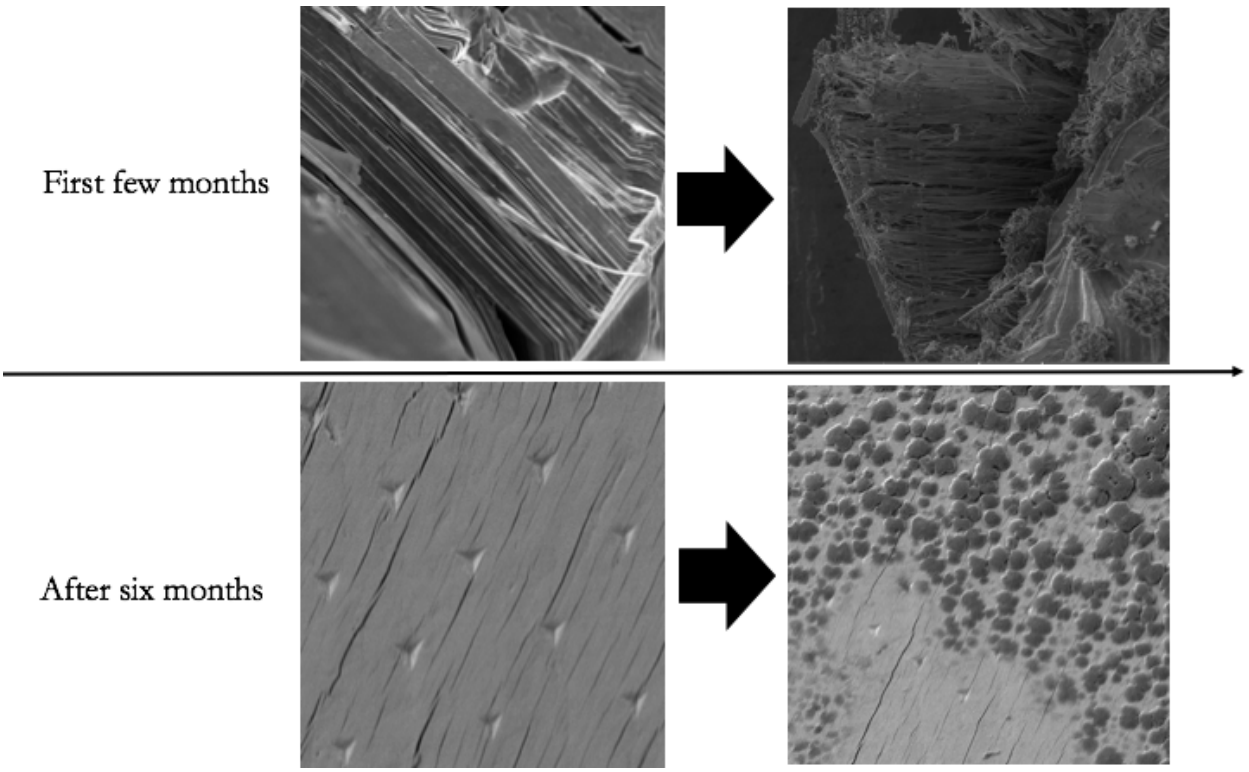

Fig. 4.10 SEM images showing the aging phenomena of $Na_{0.7}CoO_2$

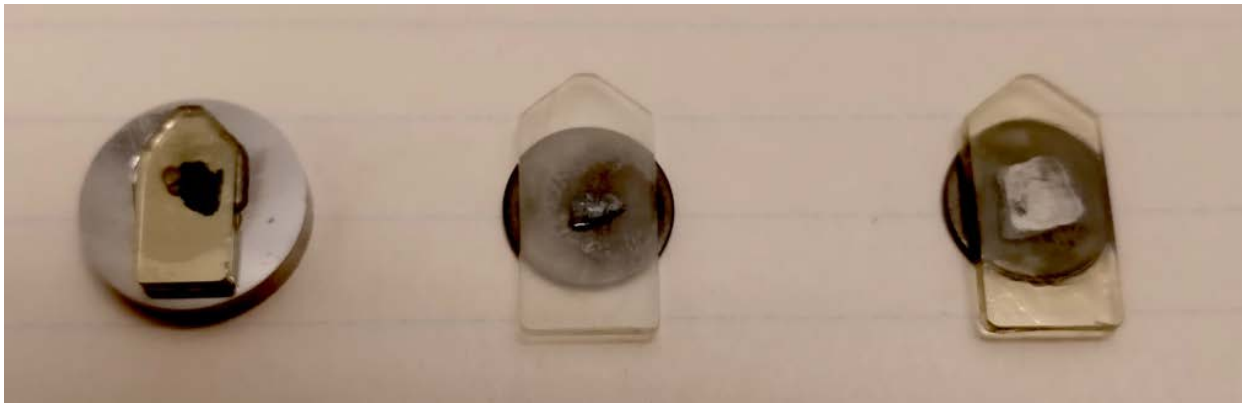

Fig. 4.1 A picture of the samples surface under aging effect. The one on the left is a “new” sample, the one in the middle is a sample which is made 6 months ago, and the one on the right is a sample made over a year ago.

One possible explanation is the shrinking of the nanolayers that causes the crack to happen between layers. Another possibility is that as the materials are embedded in epoxy for better polishing results, the material might be pulled or compressed by the surrounding epoxy when environment change (storage temperature or humidity etc.). After some time, the deformation would accumulate, and the weak bonding between layers fail to connect the layers together, and delamination would happen.

The unknown surface material may be associated with the air since the samples are exposed to air after nanoindentation. The oxygen and humidity might have chemical reaction to $Na_{0.7}CoO_2$ and form other phases.

4.2.3. The Mechanism of Layer Deformation

Even though the hardness is not related to layer length, nanoindentation hardness of $Na_{0.7}CoO_2$ samples varies within the range from 1.3 GPa to 2.1 GPa. To understand the cause of the difference in hardness between samples, two samples were carefully studied. One of them has a relatively high hardness (~2 GPa), while the other one has a relative low hardness (~1.3 GPa). SEM images along with SFM images are shown for both samples. For the sample on the left, pile-up in all three directions is observed. The pile-up is different from the edge to the center (tip of the indenter). The outer part of the pile-up is connected to the surface, while the ones close to the center shows cracks and spalling. A similar phenomenon is observed in another sample. The difference is that the pile-up of the other sample is accumulated in one direction instead of uniformly formed. Wrinkling, cracks and spalling are all in the SEM image. A continuous crack is formed around the pile-up.

The different pile-up can be explained by the varied layer orientation under the indenter. For sample A, as the force is perpendicular to the layer orientation, it is evenly distributed in every direction. As a result, the pile-up is distributed evenly in three directions. For sample B, the layers are tilted to one direction, so the pile up is more distributed in certain directions than others. The different layer orientation also explains the different hardness of two samples.

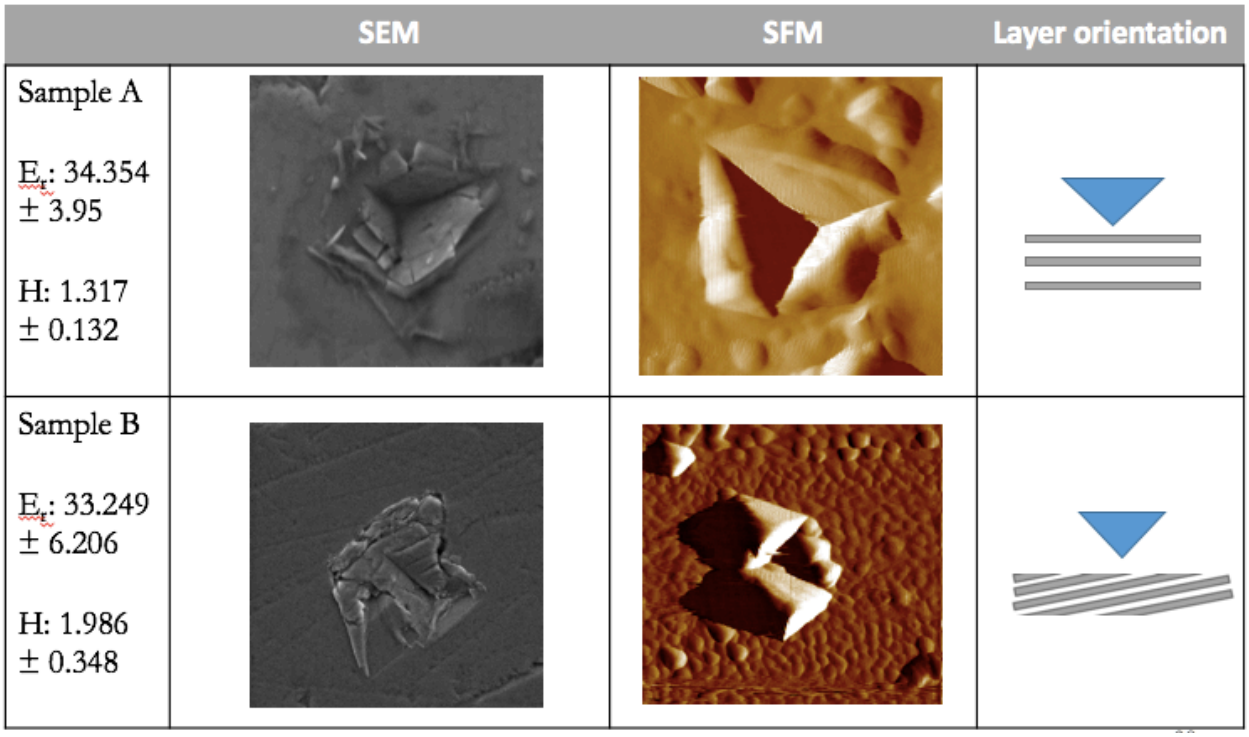

Fig. 4.12 The SEM and SFM images of two samples, along with their layer orientation under the indenter. The upper row belongs to sample A with small hardness, and the right one is sample B with large hardness.

The typical load-displacement curves of indentations made on $Na_{0.7}CoO_2$ samples with maximum load (1000 μN) are shown in Fig. 4.13. The load-displacement curves of indentations made on both samples are mostly smooth, but there are few sudden displacement jumps during loading process in both curves. The sudden displacement jump is called “pop-in”. “Pop-in” also

happens in other layered structure materials like Teflon-AF nanosheets [83], and is explained by the “tablet sliding” theory. The sliding of layers is said to happen when the indenter reaches the tablet interfaces.

The “tablet sliding” theory can also explain the deformation of $Na_{0.7}CoO_2$. In Fig. 4.14, a SEM of the indent is shown. There are two regions in the “pile-up”: the buckled region, the spalling region. The buckled region is when the layer displays flexibility, and form wrinkles on the surface under compression force (by the indenter). The spalling region are full of broken sheets, as shown by the clear sharp edges in Fig. 4.14.

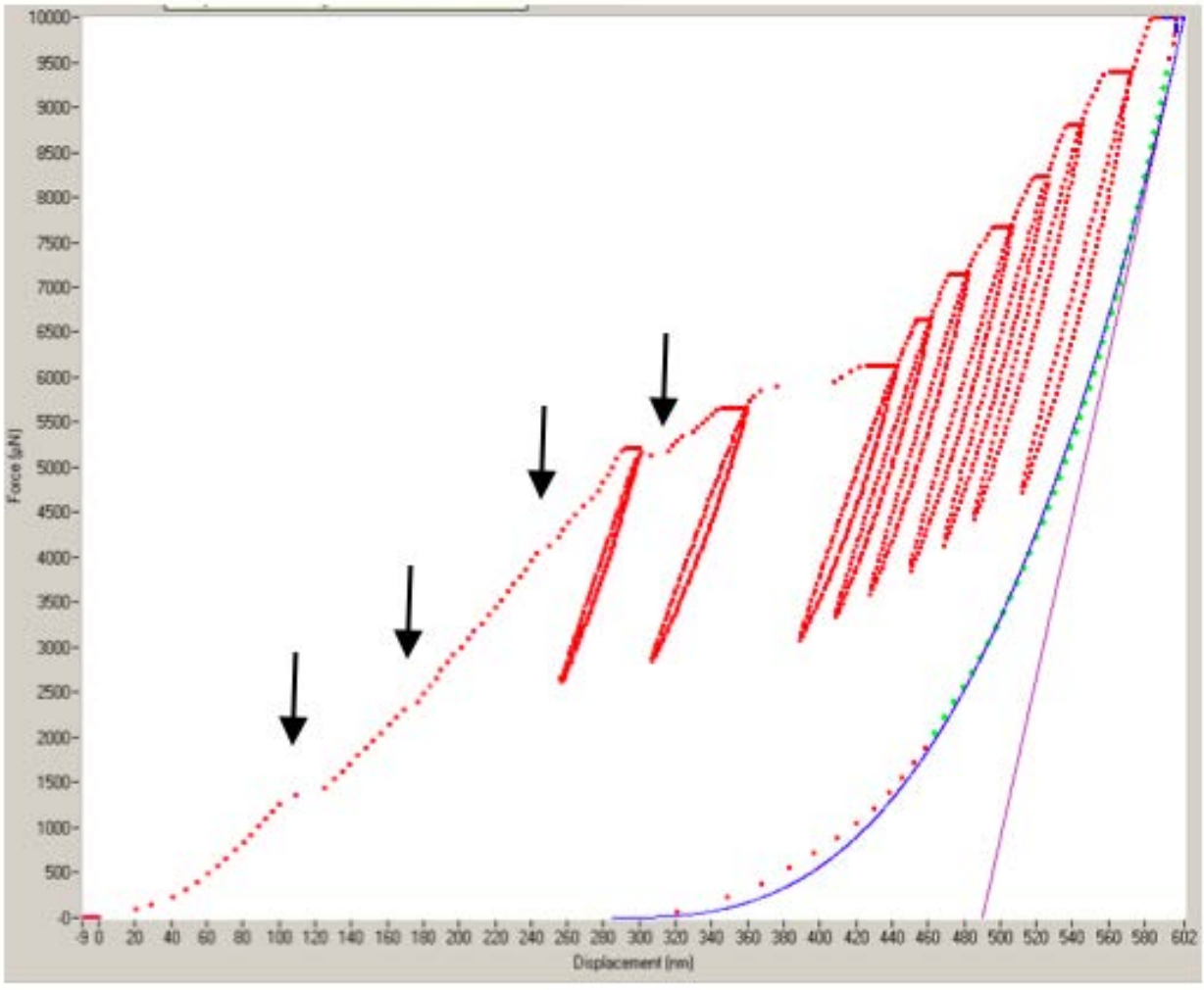

Fig. 4.13 Pop-in observed from a typical load-displacement curve from one indent on the sample

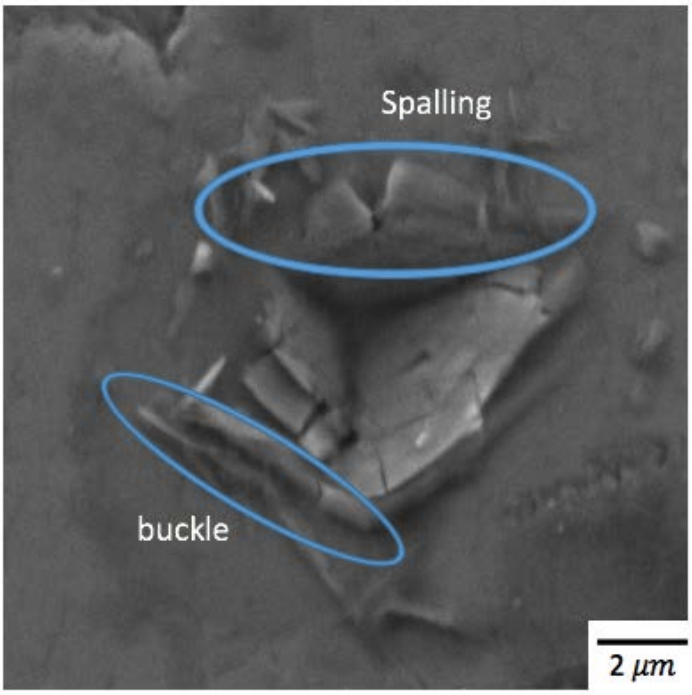

Fig. 4.14 A SEM image of a typical indent on $Na_{0.7}CoO_2$ surface

The SEM image of deformation of the layers and the "pop-in" phenomenon in the load-displacement curve gives us evidence to suggest a mechanism for the deformation of $Na_{0.7}CoO_2$. There exist four stages in the deformation of layers: (1) when the indenter reaches the first layer, the layer starts to form cracks under high stress. (2) When the indenter reaches the first interface between layers, the layer starts to slide from the stack, causing buckling and delamination from the layer below. The buckling of the layer proves the deformability of the layers. (3) As the indenter keeps moving down, more there are larger area of layer starting to buckle. (4) The layer can't dissipate the stress, the part of the layer which is close to the indenter start to spall. (5) The same effect repeats itself for each layer.

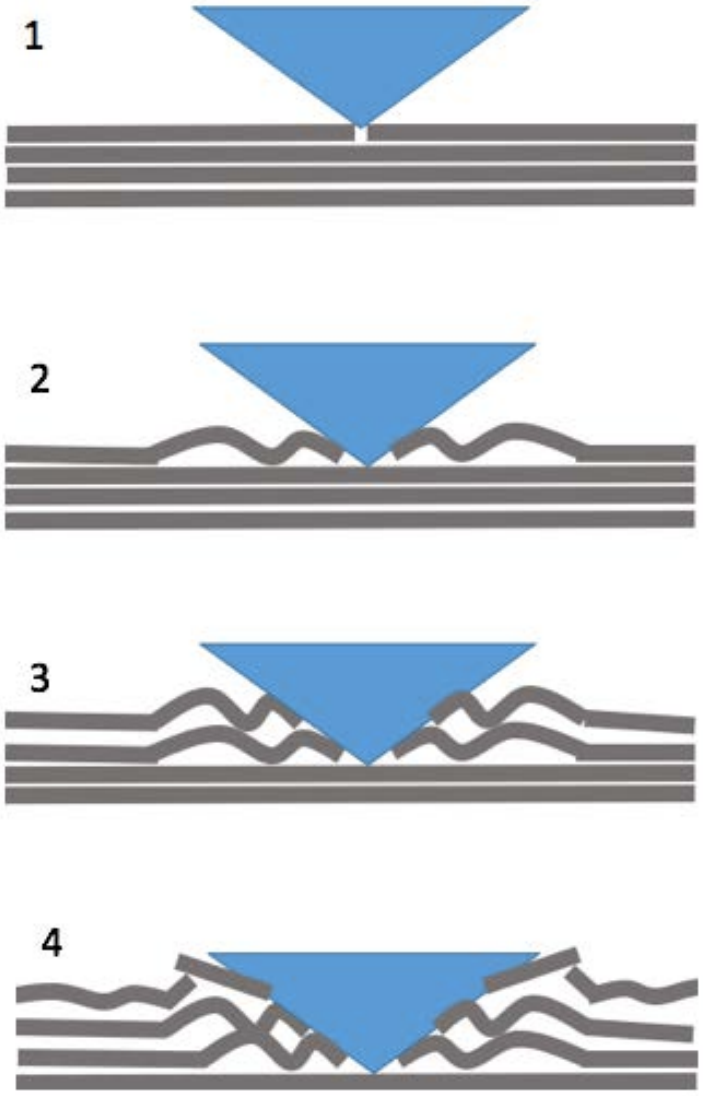

Fig. 4. 15 Schematic of various stages in nanoindentation fracture on one layer

In the first stage, the contact area is very small, thus high stress is applied to the contact area. The crack would start to form under the indent. As the indenter reaches the interface, the layer starts to slide away from the indenter tip, and the sudden sliding of layers caused a periodic “pop-in” in the load-displacement curve. Under a certain pressure, the part of layer which is around the indenter starts to buckle due to flexibility of the layer itself under high lateral

pressure. The theory of buckling has been studied by several researchers [84-86]. As the stress is accumulating, high stress applied on the edge of the buckled layers causes the separated layers to spall. As the indenter goes deeper, the height of bulged layer increase.

5. Summary and conclusions

In this study, the bulk $Na_{0.7}CoO_2$ is studied. The mechanism of demixing is studied by examining the influence of temperature, currents and duration of demixing on the formation of nanosheets. A new mechanism to explain the layer deformation under indentation base on layer sliding of buckling is reported. The fragility of the layer interface was proven by the delamination during mechanical polishing. Aging of the sample, which includes the morphology change and compositional change is first reported for $Na_{0.7}CoO_2$. The aging has two steps. The first step is the structural change by forming cracks and delamination of layers, and the second step is compositional change in the sample surface due to air exposure. The hardness and elastic modulus data based on nanoindentation tests are reported in this work for the first time. The elastic modulus of this material is around 33 GPa, and the hardness ranges from 1.25 to 2 GPa depending the different layer orientation.

6. References

[1] V. Nicolosi, M. Chhowalla, M. G. Kanatzidis, M. G, M. S. Strano, J. N. Coleman, “Liquid exfoliation of layered materials,” Science, 2013, 340, 1420.

[2] S. Wang, S. Yata, J. Nagano, Y. Okano, H. Kinoshita, H. Kikuta, and T. Yamabe, “A new carbonaceous material with large capacity and high efficiency for rechargeable Li-ion batteries,” Journal of the Electrochemical Society, 2000, 147, 2498.

[3] K. S. Novoselov, A. K. Geim, S. V. Morozov, D. Jiang, Y. Zhang, S. V. Dubonos, I. V. Grigorieva, A. A. Firsov, “Electric field effect in atomically thin carbon films,” Science, 2004, 306, 666.

[4] G. Fiori, F. Bonaccorso, G. Iannaccone, T. Palacios, D. Neumaier, A. Seabaugh, S. K. Banerjee, and L. Colombo, “Electronics based on two-dimensional materials,” Nature Nanotechnology, 2014, 9, 768.

[5] A. Molle, J. Goldberger, M. Houssa, Y.Xu, S. C. Zhang, and D. Akinwande, “Buckled two-dimensional Xene sheets,”, Nature Materials, 2017, 16, 163.

[6] C. L. Tumbade, G. R. Dhokane, “Graphene Uses & Applications,” Indian Journal of Science, 2015, 4, 4-6.

[7] M. Osada and T. Sasaki, “Exfoliated oxide nanosheets: new solution to nanoelectronics,” Journal of Materials Chemistry, 2009, 19, 2503–2511.

[8] J. N. Coleman, M. Lotya, A. O’Neill, S. D. Bergin, P. J. King, U. Khan, K. Young, A. Gaucher, S. De, R. J. Smith, I. V. Shvets, S. K. Arora, G. Stanton, H.-Y. Kim, K. Lee, G. T. Kim, G. S. Duesberg, T. Hallam, J. J. Boland, J. J. Wang, J. F. Donegan, J. C. Grunlan, G. Moriarty, A. Shmeliov, R. J. Nicholls, J. M. Perkins, E. M. Grieveson, K. Theuwissen, D. W.

McComb, P. D. Nellist and V. Nicolosi, “ Two-demensional nanosheets produced by liquid exfoliation of layered materials, ” Science, 2011, 331, 568.

[9] R. Ma and T. Sasaki, “Nanosheets of oxides and hydrooxides: Ultimate 2D charge-bearing functional crystallites” Advanced Materials, 2010, 22, 5082.

[10] A. Takagaki, M. Sugisawa, D. Lu, J. N. Kondo, M. Hara, K. Domen and S. Hayashi, “Exfoliated nanosheets as a new strong solid acid catalyst,” Journal of the American Chemical Society, 2003, 125, 5479.

[11] L. Z. Wang, K. Takada, A. Kajiyama, M. Onoda, Y. Michiue, L. Q. Zhang, M. Watanabe and T. Sasaki, “Synthesis of a Li−Mn-oxide with disordered layer sacking through flocculation of exfoliated MnO2 nanosheets, and its electrochemical properties,” Chemistry of materials, 2003, 15, 4508.

[12] I. Terasaki, Y. Sasago, and K. Uchinokura, “Large thermoelectric power in $NaCo_2O_4$ single crystals,” Physical Review Letters B, 1997, 56, 12685.

[13] A. Bhide and K. Hariharan, “Physicochemical properties of Na_xCoO_2 as a cathode for solid state sodium battery,” Solid State Ionics, 2011, 192, 360.

[14] L.W. Shacklette, T.R. Jow, L. Townsend, “Rechargeable electrodes from sodium cobalt bronzes,” Journal of Electrochemical Society, 1988, 135, 2671.

[15] M.M. Doeff, S.J. Visco, Y. Ma, M. Peng, L. Ding, L.C.D. Jonghe, “Thin film solid state sodium batteries for electric vehicles,” Electrochimica Acta, 19945, 40, 2205.

[16] D.A. Stevens, J.R. Dahn, “High capacity anode materials for rechargeable sodium-ion batteries,” Journal of The Electrochemical Society, 2000, 147, 1271.

[17] K. K. Sanjeev, Y. Zhang, S. P. Baker, and R. D. Robinson, "A study on the scalable synthesis of ductile 2-D nanosheets of thermoelectric Na_xCoO_2."

[18] I. Terasaki, I. Tsukada and Y. Iguchi. "Impurity-induced transition and impurity-enhanced thermopower in the thermoelectric oxide $NaCo_{2-x}Cu_xO_4$," Physical Review B, 2002, 65, 195106.

[19] M. Aksit, D. P. Toledo, and R. D. Robinson, "Salable nanomanufacturing of millimeter-length 2D Na_xCoO_2 nanosheets," Journal of Materials Chemistry, 2012, 22, 5936.

[20] C. G. Andres, P. Menno, and S. Steele, Gary, "Elastic properties of freely suspended MoS_2 nanosheets," Advanced Materials, 2012, 24, 772.

[21] B. Radisavljevic, A. Radenovic, J. Brivio, V. Giacometti, A. Kis, "Single-layer MoS_2 transistors," Nature Nanotechnology, 2011, 6, 147–150.

[22] H. Li, J. Wu, Z. Yin, H. Zhang, "Preparation and applications of mechanically exfoliated single-layer and multilayer MoS_2 and WSe_2 nanosheets," Accounts of Chemical Research, 2014, 47, 1067.

[23] B. J. Kim, H. Jang, S. K. Lee, B. H. Hong, J. H. Ahn, J. H.; Cho, "High-performance flexible graphene field effect transistors with ion gel gate electrics," Nano Letter, 2010, 10, 3464–3466.

[24] S. K. Lee, B. J. Kim, H. Jang, S. C. Yoon, C. Lee, B. H. Hong, J. A. Rogers, J. H. Cho, J. H. Ahn, "Stretchable graphene transistors with printed dielectrics and gate electrodes," Nano Letter, 2011, 11, 4642.

[25] T. M. Tritt, and M. A. Subramanian, "Thermoelectric materials, phenomena, and applications: A bird 's eye view," MRS Bulletin, 2006, 31, 188.

[26] R. Ray, A. Ghoshray, and K. Ghoshray, "^{59} Co NMR studies of metallic $NaCo_2O_4$,"

Physical Review Letters B, 1999 59, 9454.

[27] K. Takada, H. Sakurai, E. Takayama–Muromachi, F. Izumi, R. A. Dilanian, and T. Sasaki, "Superconductivity in two-dimensional CoO_2 layers," Nature, 2003, 422, 53–55.

[28] C. Fouassier, G. Matejka, J. M. Reau, P. Hagenmuller, "Sur de nouveaux bronzes oxygénés de formule $Na_\chi CoO_2$. Le système cobalt-oxygène-sodium," Journal of Solid State Chemistry, 1973, 6, 532.

[29] H.Yakabe, H.Kikuchi, I.Terasaki, Y.Sasago and K.Uchinokura, "Thermoelectric Properties of Transition-Metal Oxide $NaCo_2O_4$ System," Proc. 16th Int. Conf. Thermoelectrics, IEEE, Piscataway, 19985, 23.

[30] Y. Ono, R. Ishikawa, Y. Miyazaki, Y. Ishii, Y. Morii, T. Kajitani, "Crystal structure, electric and magnetic properties of layered cobaltite β-Na_xCoO_2," Journal of Solid State Chemistry, 2002, 166.

[31] M. L. Foo, Y. Wang, S. Watauchi, H. W. Zandbergen, T. He, R. J. Cava, and N. P. Ong, "Charge ordering, commensurability, and metallicity in the phase diagram of the layered Na_xCoO_2," Physical Review Letters, 2004, 92, 247001.

[32] H. W. Zandbergen, M. Foo, Q. Xu, V. Kumar, and R. J. Cava, "Sodium ion ordering in Na_xCoO_2: Electron diffraction study," Physical Review Letters B, 2004, 70, 024101.

[33] Q. Huang, M. L. Foo, J. W. Lynn, H. W. Zandbergen, G. Lawes, Yayu Wang, B. H. Toby, A. P. Ramirez, N. P. Ong, and R. J. Cava, "Low temperature phase transitions and crystal structure of $Na_{0.5}CoO_2$," Journal of Physics: Condensed Matter, 2004, 16, 5803.

[34] X. Yan, B. Poudel, Y. Ma, W. S. Liu, G. Joshi, H. Wang†, Y. Lan†, D. Wang, G. Chen and

Z. F. Ren, “Experimental Studies on Anisotropic Thermoelectric Properties and Structures of n-Type $Bi_2Te_{2.7}Se_{0.3}$,” Nanoletters, 2010, 10, 3373.

[35] Y.G. Shi, Y.L. Liu, H.X. Yang, C.J. Nie, R. Jin, and J.Q. Li, “Raman spectroscopy study of Na_xCoO_2 and superconducting $Na_xCoO_2 \cdot yH_2O$,” Physical Review B, 2004, 70, 052502.

[36] M. Ito, T. Nagira, Y. Tsuchiya, S. Katsuyama, K. Majima, andH. Nagai, “Microstructure and thermoelectric properties of $Na_xCo_2O_4$ synthesized by spark plasma sintering,” Journal of Japan Society of Powder, 2002, 49, 406.

[37] M. Ito, T. Nagira, D. Furumoto, Y. Odal, and S. Hara, “Synthesis of $NaxCo_2O_4$ thermoelectric oxide with crystallographic anisotropy by chemical solution process,” Science and Technology of Advance Materials, 2004, 5, 125.

[38] W.T. Petuskey, and H.K. Bowen, “Thermal segregation of cations in iron Aluminate spinels,” Journal of American Ceramic Society, 1981, 64, 611.

[39] H. Schmalzried, W. Laqua, and P.L. Lin Z. “Crystalline oxide solid solutions in oxygen potential gradients,” Naturforsch, 1979, 34, 192.

[40] H. Schmalzried, and W. Laqua, “Multicomponent oxides in oxygen potential gradients,” Oxidation of Metals, 1981, 15, 339.

[41] M. Martin, and R. Schmackpfeffer, “Demixing of doped oxides: influence of defect interactions,” Solid State Ionics, 1994, 72, 67.

[42] C.C. Wang, K.S. Goto, and S.A. Akbar, “Demixing of (Ni, Co) O under an oxygen potential gradient using a YSZ-based galvanic cell” Journal of The Electrochemical Society,” 1991, 138, 3673.

[43] D. Dimos, J. Wolfenstein, and D.L. Kohlstedt, “Kinetic demixing and decomposition of multicomponent oxides due to a nonhydrostatic stress,” Acta Mettalurgica, 1988, 36, 1543.

[44] D. Monceau, M. Filal, M. Tebtoub, C. Petot, and G. Petot-Ervas, “Kinetic demixing of ceramics in an electrical field,” Solid State Ionics, 1994, 73, 221.

[45] H.I. Yoo, and K. C. Lee, “Equal mobility of constituent cations in $BaTiO_3$,” Applied Physics Letter, 2008, 92, 252103.

[46] M. Schnehage, R. Dieckmann and H. Schmalzried, “Point defects in oxide solid solutions (IV). Correlated diffusion of cations and vacancies in (Co, Mg)O-mixed crystals,” Physical Chemistry Chemical Physics, 1982, 86, 1061.

[47] H. Ohta, S. W. Kim, S. Ohta, K. Koumoto, M. Hirano and H. Hosono, “Reactive solid-phase epitaxial growth of Na_xCoO_2 (x~ 0.83) via lateral diffusion of Na into a cobalt oxide epitaxial layer “Crystal Growth and Design, 2005, 5, 25.

[48] Y. Tsori, F. Tournihac, and L. Leibler, “Demixing in simple fluids induced by electric field gradients,” 2004, 430, 544.

[49] O. Teller, and M. Martin, “Kinetic demixing of (Co,Ni)O in an electric field,” Solid State Ionics, 1997, 101-103, 475.

[50] Q. L. Wu, A. O. Sjastad, B. Vistad, K. D. Knudsen, J. Roots, J. S. Pedersen, and P. Norby, “Characterization of exfoliated layereddouble hydroxide (LDH, Mg/Al=3) nanosheets at highconcentrations in formamide,” Journal of Materials Chemistry, 2007, 17, 965.

[51] K. J. Coyne, X. X. Qin, and J. H. Waite, “Extensible collagen in mussel byssus: a natural block copolymer,” Science, 1997, 277, 1830-1832.

[52] J. D. Currey, and J. Biomech. “Mechanical properties of bone tissues with greatly differing

functions," 1979, 12, 313.

[53] J. D. Currey, "Mechanical properties of mollusc shell," Society of Experimental Biology, 1980, 34, 75.

[54] R. Z. Wang, Z. Suo, A. G. Evans, N. Yao, and I. A. Aksay, "Deformation mechanisms in nacre," Journal of Materials Research, 2001, 16, 2485.

[55] Heslot, and H. Biochimie, "Artificial fibrous proteins: a review," 1998, 80, 19.

[56] G. S. Decher, "Fuzzy Nanoassemblies: Toward layered polymeric multicomposites," Science, 1997, 277, 1232.

[57] A. K. Geim, "Graphene: Status and prospects," Science, 2009, 324, 1530.

[58] A. K. Geim, and K. S. Novoselov, "The rise of graphene," Nature Materials, 2007, 6, 183-191.

[59] K. S. Novoselov, V. I. Fal′ko, L. Colombo, P. R. Gellert, M. G. Schwab, and K. Kim, "A roadmap for graphene," Nature, 2012, 490, 192.

[60] R. Z. Ma, and T. Sasaki, "Nanosheets of oxides and hydroxides: Ultimate 2D charge-bearing functional crystallites," Advanced Materials, 2010, 22, 5082

[61] M. D. Ventra, S. Evoy, and J. R. Heflin, "Introduction to nanoscale science and technology," Springer Science and Business Media.

[62] M. Osada, and T. Sasaki, "Exfoliated oxide nanosheets: New solution to nanoelectronics," Journal of Materials Chemistry, 2009, 19, 2503.

[63] M. Osada, and T. Sasaki, "Two-dimensional dielectricnanosheets: Novel nanoelectronics from nanocrystal building blocks," Advaned Materials, 2012, 24, 210.

[64] M. A. Bizeto, A. L. Shiguihara, and V. R. L. Constantino, “Layered Niobate nanosheets: Building blocks for advanced materials assembly,” Journal of Materials Chemistry, 2009, 19, 2512.

[65] Z. H. Liu, K. Ooi, H. Kanoh, W. P. Tang, and T. Tomida, “Swelling and delamination behaviors of Birnessite-type manganese oxide by intercalation of Tetraalkylammonium ions,” 2000, 16, 4154.

[66] G. S. Decher, “Fuzzy Nanoassemblies: Toward layered polymeric multicomposites,” Science, 1997, 277, 1232.

[67] Z. Tang, N. A. Kotov, S. Magonov, and B. Ozturk, “Nanostructured artificial nacre,” Nature Materials, 2003, 2, 413.

[68] P. Podsiadlo, A. K. Kaushik, E. M. Arruda, A. M. Waas, B. S. Shim, J. D. Xu, “Ultrastrong and stiff layered polymer nanocomposites,” Science, 2007, 318, 80.

[69] L. J. Bonderer, A. R. Studart, and L. J. Gauckler, “Bioinspired design and assembly of platelet reinforced polymer films,” Science, 2008, 319, 1069.

[70] F. A. Bergaya, “Layered clay minerals. Basic research and innovative composite applications,” 2008, 107, 141.

[71] W. S. Hummers, and R. E. Offeman, “Preparation of Graphitic Oxide,” Journal of American Chemistry Society, 1958, 80, 1339.

[72] A. Okada, M. Kawasumi, A. Usuki, Y. Kojima, T. Kurauchi, and O. Kamigaito, “Nylon 6–Clay Hybrid,” Materials Research Society, 1990, 171, 45.

[73] X. D. Li, H. Gao, C. J. Murphy, L. Gou L, “Nanoindentation of Cu_2O nanocubes,” Nano Letters, 2004, 4, 1903.

[74] B. Bhushan, and X. Li, “Nanomechanical characterisation of solid surfaces and thin films,” International Materials Reviews, 2003, 48, 125.

[75] X. Tao, X. Wang, and X. D. Li, “Nanomechanical characterization of one-step combustion-synthesized $Al_4B_2O_9$ and $Al_{18}B_4O_{33}$ nanowires,” Nano Letters, 2007, 7, 3172.

[76] S. Suresh, T. G. Nieh, and B.W. Choi, “Nanoindentation of copper thin films on silicon substracte,” Scripta Materialia, 1999, 41, 951.

[77] U. Ramamurty, “Nanoindentation for probing the mechanical behavior of molecular crystals–a review of the technique and how to use it,” Journal of Crystal Engineer Communication, 2014, 16, 12.

[78] ASTM E10 – 14 Standard Test Method for Brinell Hardness of Metallic Materials.

[79] E. Meyer, and Z. ver. Deut. “Untersuchungenüber Härteprüfung und Härte Brinell Methoden,” Zetschrift Des Vereines Deutscher Ingenieure, 1908, 52, 645.

[80] R. L. Smith, and G.E. Sandland, “An Accurate Method of Determining the Hardness of Metals, with Particular Reference to Those of a High Degree of Hardness," Proceedings of the Institution of Mechanical Engineers, 1922, 1, 623.

[81] W. C. Oliver, G. M. Pharr, “An improved technique for determining hardness and elastic modulus using load and displacement sensing indentation experiments,” Journal of Materials Research, 1992, 7, 1564.

[82] F. Barthelat, C. M. Li, C. Comi, and H. D. Espinosa, “Mechanical properties of nacre consituents and their impact on mechanicalperformance,” Journal of Materials Research. 2011, 21, 1977.

[83] M. A. Gulgun, M. H. Nguyen, and W. M. Kriven, “Polymerized Organic-Inorganic Synthesis of Mixed Oxides,” Journal of American Ceramics Society,” 1999, 82, 556.

J. Kakihana, “Invited review “sol-gel” preparation of high temperature superconducting oxides,” Journal of Sol-Gel Science and Technology, 1996, 6, 7.

[84] D. B. Marshall, and A. G. Evans, “Adhesion measurement of thin films by indentation,” Journal of Applied Physics, 1984, 56, 2632.

[85] M. P. de Boer, H. Huang, H. and W. W. Gerberich, “In thin films: stresses and mechanical properties,” Materials Research Society Symposium Proceedings, 1997, 3, 56.

[86] D. F. Diao, and Y. Sawaki, “Fracture mechanisms of thin amorphous carbon films in Nanoindentation,” Thin Solid Films, 1995, 270, 362.